

Constraints on three flavor neutrino mixing

MOHAN NARAYAN

Department of Physics, Indian Institute of Technology, Mumbai 400 076, India

Abstract. We summarize the constraints on three flavor neutrino mixing coming from data. We first map out the allowed region in the three neutrino parameter space using solar and atmospheric neutrino data. We then incorporate the results of reactor and long baseline experiments in our analysis and show that the parameter space is drastically reduced. We conclude by pointing out that the results of Borexino and SNO will further help in constraining the parameter space.

Keywords. Neutrino; oscillations; parameters.

PACS Nos 14.60.Pq; 26.65.+t

1. Why three flavors?

- LEP data tells us that there are three light active neutrino flavors, so any realistic analysis of oscillation phenomena should incorporate all the three flavors.
- A two flavor analysis of the solar neutrino problem [1] demands a $\delta m^2 \approx 10^{-6} \text{eV}^2$ to fit data from all experiments, where δm^2 is the mass squared difference between the two mass eigenstates.
- A two flavor analysis of the atmospheric neutrino problem [2,3] demands a $\delta m^2 \approx 10^{-3} \text{eV}^2$ to fit data from all experiments, where again δm^2 is the mass squared difference between the two mass eigenstates.

Therefore to simultaneously address both the solar and the atmospheric neutrino problems, one needs a minimum of two independent mass squared differences, which three flavors naturally provides.

2. The solar neutrino problem

We briefly discuss the mixing between three flavors of neutrinos and then obtain the probability for a ν_e produced in the sun to be detected as a ν_e on earth. The three flavor eigenstates are related to the three mass eigenstates in vacuum through a unitary transformation,

$$\begin{bmatrix} \nu_e \\ \nu_\mu \\ \nu_\tau \end{bmatrix} = U^v \begin{bmatrix} \nu_1^v \\ \nu_2^v \\ \nu_3^v \end{bmatrix}, \quad (1)$$

where the superscript v on r.h.s. stands for vacuum. The 3×3 unitary matrix U^v can be parametrized by three Euler angles (ω, ϕ, ψ) and a phase. The form of the unitary matrix can therefore be written in general as

$$U^v = U_{23}(\psi) \times U(\text{phase}) \times U_{13}(\phi) \times U_{12}(\omega),$$

where $U_{ij}(\theta_{ij})$ is the mixing matrix between i th and j th mass eigenstates with the mixing angle θ_{ij} [4]. All the angles can take values between 0 and $\pi/2$. It has been shown that the expression for electron neutrino survival probability, integrated over the time of emission and of absorption, is independent of the phase and the third Euler angle ψ [5,6]. They can be set to zero without loss of generality and we have the following form for U^v

$$U^v = \begin{pmatrix} c_\phi c_\omega & c_\phi s_\omega & s_\phi \\ -s_\omega & c_\omega & 0 \\ -s_\phi c_\omega & -s_\phi s_\omega & c_\phi \end{pmatrix}, \quad (2)$$

where $s_\phi = \sin \phi$ and $c_\phi = \cos \phi$ etc. Note that one of the flavors decouples if either ω or ϕ is zero and we have a two flavor scenario. The masses of the vacuum mass eigenstates are taken to be μ_1, μ_2 and μ_3 . We define the two independent mass squared differences as $\delta_{21} = \mu_2^2 - \mu_1^2$ and $\delta_{31} = \mu_3^2 - \mu_1^2$. Without loss of generality, we can take δ_{21} and δ_{31} to be greater than zero. We take $\delta_{21} \approx 10^{-6} \text{eV}^2$ which is relevant for the solar neutrino problem, and $\delta_{31} \approx 10^{-3} \text{eV}^2$ which is relevant for the atmospheric neutrino problem. Matter effects are taken into account by incorporating the Wolfenstein term denoted by A in this analysis. In the sun A can be written as $A = 0.76 \times \rho \times E \times 10^{-7}$. Here ρ is the matter density in g/cc and E is the neutrino energy. A is in eV^2 if E is expressed in MeV. Thus we work in an approximation where $\delta_{21}, A_{\text{max}} \ll \delta_{31}$, where A_{max} is the value of A at the core of the sun.

In this approximation, one can develop an analytic expression for the electron neutrino survival probability P_{ee} [7]. We get

$$\langle P_{ee} \rangle = \sum_{i,j=1}^3 |U_{ei}^v|^2 |U_{ej}^m|^2 |\langle \nu_i^v | \nu_j^m \rangle|^2. \quad (3)$$

$|\langle \nu_i^v | \nu_j^m \rangle|^2$ is the probability that the j th matter dependent eigenstate evolves into i th vacuum eigenstate. As in the two flavor case, if the adiabatic approximation holds, then

$$|\langle \nu_i^v | \nu_j^m \rangle|^2 = \delta_{ij}. \quad (4)$$

We introduce the jump probabilities

$$x_{ij} = |\langle \nu_i^v | \nu_j^m \rangle|^2 \text{ for } i \neq j \quad (5)$$

to take into account the non-adiabatic transitions, if the adiabatic condition does not hold.

The matter dependent mixing angles can be expressed in terms of the vacuum parameters and A as

$$\tan 2\omega_m = \frac{\delta_{21} \sin 2\omega}{\delta_{21} \cos 2\omega - A \cos^2 \phi}, \quad (6)$$

Constraints on three flavor neutrino mixing

$$\sin \phi_m = \sin \phi \left[1 + \frac{A}{\delta_{31}} \cos^2 \phi \right]; \quad \cos \phi_m = \cos \phi \left[1 - \frac{A}{\delta_{31}} \sin^2 \phi \right]. \quad (7)$$

The matter dependent eigenvalues m_i^2 are given by

$$\begin{aligned} m_1^2 &= A \cos^2 \phi \cos^2 \omega_m + \delta_{21} \sin^2 (\omega - \omega_m), \\ m_2^2 &= A \cos^2 \phi \sin^2 \omega_m + \delta_{21} \cos^2 (\omega - \omega_m), \\ m_3^2 &= \delta_{31} + A \sin^2 \phi \simeq \delta_{31}. \end{aligned} \quad (8)$$

ω_m can undergo a resonance if the values of δ_{21} , ϕ and ω are such that the resonance condition

$$A(r) \cos^2 \phi = \delta_{21} \cos 2\omega \quad (9)$$

is satisfied for some r [4]. Note that this condition is very similar to the resonance condition in the two flavor case

$$A(r) = \delta_{21} \cos 2\omega.$$

The new feature here, which occurs due to the mixing among the three neutrino flavors, is the presence of the second mixing angle ϕ in the resonance condition. This dependence on ϕ leads to a larger region of allowed parameter space in the three flavor oscillation scenario as will be shown in the next later.

Because $\delta_{31} \gg A_{\max}, \delta_{21}$, the third eigenvalue, both in vacuum and in matter, is much larger than the other two eigenvalues. Non-adiabatic effects are significant only if the eigenvalues of two states come close together [8]. Therefore the jump probabilities involving the third state, x_{13} and x_{23} are expected to be negligibly small. Thus we have the expression for electron neutrino survival probability to be

$$\begin{aligned} \langle P_{ee} \rangle &= \cos^2 \phi \cos^2 \phi_m (\cos^2 \omega \cos^2 \omega_m + \sin^2 \omega \sin^2 \omega_m) \\ &\quad + \sin^2 \phi \sin^2 \phi_m - x_{12} \cos^2 \phi \cos^2 \phi_m \cos 2\omega \cos 2\omega_m. \end{aligned} \quad (10)$$

For x_{12} we use the formula,

$$x_{12} = \frac{\exp\left[-\frac{\pi\gamma F}{2}\right] - \exp\left[-\frac{\pi\gamma F}{2\sin^2\omega}\right]}{1 - \exp\left[-\frac{\pi\gamma F}{2\sin^2\omega}\right]}, \quad (11)$$

where γ is defined as

$$\gamma \equiv \frac{\delta_{21}}{2E} \left| \frac{1}{A} \frac{dA}{dr} \right|_{res} \frac{\sin^2 2\omega}{\cos 2\omega}. \quad (12)$$

γ is known as the adiabaticity parameter, and it gives us a criterion for estimating the non-adiabatic effects during the propagation of the neutrino. If $\gamma \gg 1$, then non-adiabatic effects are negligible and the propagation is essentially adiabatic. On the other hand $\gamma \approx 1$ means there can be substantial corrections to the adiabatic approximation. Note that γ is evaluated at the resonance point, that is because non-adiabatic effects are important only in the vicinity of the resonance. The function F depends upon the density profile in which the neutrino propagates, and

$$F = 1 - \tan^2 \omega \quad (13)$$

for an exponentially varying solar density [4] as in the case of the sun. We use eq. (11) for the jump probability since it is valid both for large and small mixing angles. In the extreme non-adiabatic limit $x_{12} \rightarrow \cos^2 \omega$ and when $\gamma F \gg 1$, we have the usual Landau–Zener jump probability given by $x_{12} \rightarrow \exp(-\pi\gamma F/2)$ [4] as expected. We use the expression for $\langle P_{ee} \rangle$ in (10) and find the ranges of δ_{21} , ω and ϕ allowed by the three solar neutrino experiments. Since $\delta_{31} \gg A_{\max}$, we see from the expression for ϕ_m in (7) that the angle ϕ is almost unaffected by the matter effects. However, ω_m can be significantly different from ω and can undergo resonance if the resonance condition in (9) is satisfied. Since this resonance condition depends on ϕ , in addition to δ_{21} and ω , a larger region of parameter space satisfies the three constraints from the experiments.

2.1 Results and conclusions

To search for the regions allowed in the three parameter space δ_{21} , ω and ϕ , we define the suppression factors observed by the four types of experiments

$$y_{\text{Ga}} = \frac{R_{\text{Ga};\text{avg}}}{R_{\text{Ga};\text{SSM}}} = 0.544 \pm 0.074,$$

$$y_{\text{Cl}} = \frac{R_{\text{Cl}}}{R_{\text{Cl};\text{SSM}}} = 0.2731 \pm 0.044,$$

$$y_{\text{Kam}} = \frac{R_{\text{Kam}}}{R_{\text{Kam};\text{SSM}}} = 0.423 \pm 0.058, \quad (14)$$

$$y_{\text{SKam}} = \frac{R_{\text{SKam}}}{R_{\text{SKam};\text{SSM}}} = 0.379 \pm 0.034, \quad (15)$$

where the first number refers to the average of the data given by two experiments – namely GALLEX [9] and SAGE [10]. The number for the chlorine experiment is from ref. [11]. Kamioka and super-Kamioka data are taken from refs [12] and [13] respectively. The predicted SSM rates for various experiments were taken from Bahcall–Pinsonneault SSM calculations [14]. The uncertainties in y_i are the sum of the experimental uncertainty in the numerator and the theoretical uncertainty in the denominator, added in quadrature. Because of its different threshold, we treat super-Kamioka as a different experiment.

The predictions for y_i for the three flavor oscillation scenario are obtained by convoluting the SSM fluxes and the detector cross sections with $\langle P_{ee} \rangle$ from (10). The expression we use is

$$y = \frac{\sum_K \int_{E_{\min}}^{E_{\max}} dE \Phi_K(E) \sigma(E) \langle P_{ee} \rangle (E)}{\sum_K \int_{E_{\min}}^{E_{\max}} dE \Phi_K(E) \sigma(E)}, \quad (16)$$

where the sum over K refers to the neutrino fluxes from various sources contributing to the process. We also include the contributions from the CNO cycle apart from the dominant contributions from the $p-p$ cycle. In the case of Kamioka, and super-Kamioka only the ^8B flux contributes and one must also take into account the neutral current contribution arising from the muon and tau neutrinos interacting with the detector material. The parameter

ranges are then calculated by putting vetos on y at 1.6σ levels. The energy dependent fluxes were taken from ref. [14] and the cross sections were taken from ref. [15].

We show the results in figure 1 as regions allowed at 90 per cent C.L in the $\omega - \delta_{21}$ plane, for various values of ϕ . The following features emerge from the graphs.

1. The panel labelled (a) shows the region allowed for $\phi = 0^\circ$. There are two distinct regions in the parameter space. The first region has $\delta_{21} < 10^{-5} \text{eV}^2$, and ω about

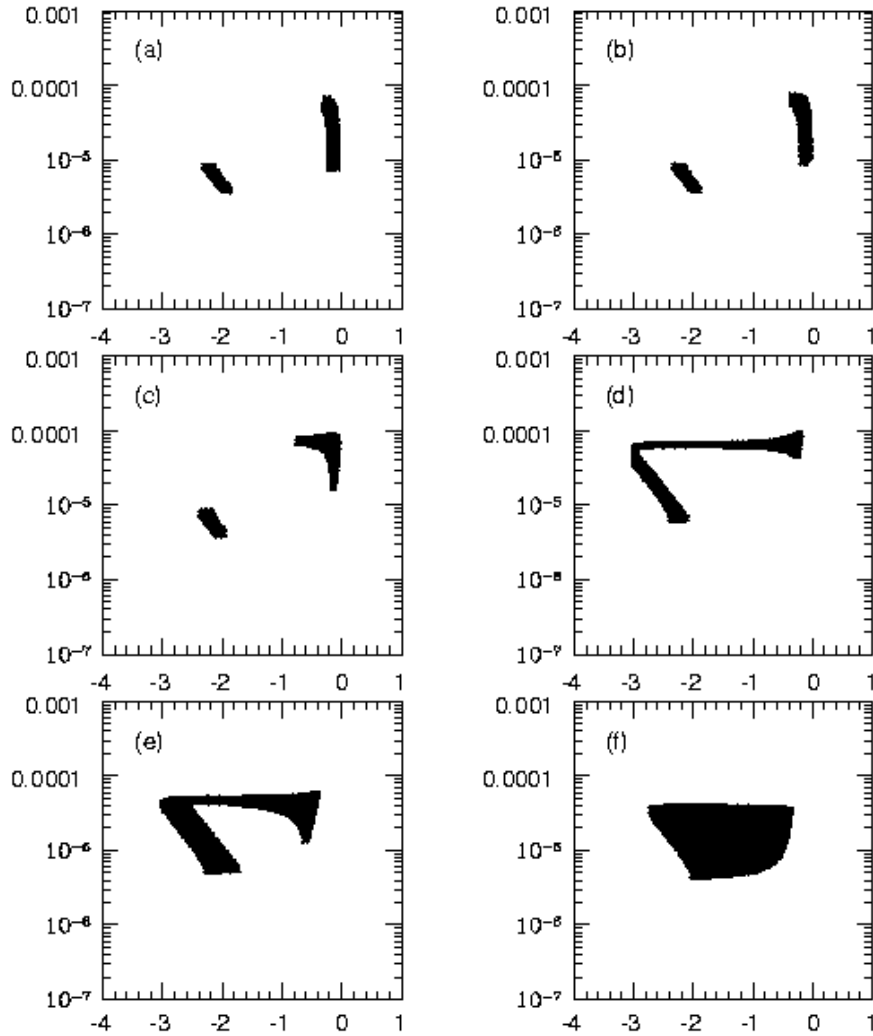


Figure 1. Allowed regions in the ω - δ plane for various values of ϕ . The x -axis shows $\log(\sin^2 \theta)$ and the y -axis δ_{21} in eV^2 .

- 3°. This is called the small angle region. The other region has $\delta_{21} > 10^{-5} \text{eV}^2$, and $\omega > 25^\circ$. This is called the large angle region. Notice the clear separation between the two regions.
2. Panel (b) shows the region allowed for $\phi = 10^\circ$. One sees that there is no perceptible difference, when compared to the $\phi = 0^\circ$ case.
 3. Panel (c) shows the region allowed for $\phi = 20^\circ$. Now the value of ϕ starts influencing the parameter space. The small angle region is almost the same, while the large angle region broadens a bit to include slightly smaller values of ω .
 4. Panel (d) shows the region allowed for $\phi = 30^\circ$. Now both the small angle as well as the large angle regions broaden, and they almost merge at a point. Each region has the appearance of two limbs.
 5. Panel (e) shows the region allowed for $\phi = 40^\circ$. The two limbs merge with each other at one end of each limb. But one can still discern the two different limbs.
 6. Panel (f) shows the region allowed for $\phi = 45^\circ$. Now two limbs completely merge with each other, and there is one single patch in the parameter space. Hence the effect of increasing ϕ is finally to merge the two disjoint regions into one single region.

Note that the parameter space obtained in the present analysis, is more or less the same parameter space which was obtained in previous analyses of solar neutrino problem in three flavors using older data [7,16].

The various regions of the allowed parameter space may be classified as follows:

1. small δ_{21} , small ω , small ϕ ,
2. large δ_{21} , large ω , small ϕ ,
3. small δ_{21} , small ω , large ϕ ,
4. large δ_{21} , small ω , large ϕ ,
5. large δ_{21} , large ω , large ϕ ,

where the small or large δ_{21} means either $\delta_{21} < 10^{-5} \text{eV}^2$ or $\delta_{21} > 10^{-5} \text{eV}^2$. The first two regions corresponding to small ϕ in the above classification belong to an approximate two generation situation since the angle ϕ is small. The one corresponding to small ω is the usual non-adiabatic solution, whereas the one corresponding to large ω is the usual adiabatic solution. The rest invoke the genuine three generation oscillation mechanism. In conclusion the solar neutrino problem enables us to put bounds on three of the five parameters which occur in neutrino mixing.

3. The atmospheric neutrino problem

The atmosphere is a source of electron as well as muon type of neutrinos and antineutrinos. These neutrinos are the end product of a cascade process which is triggered by cosmic rays interacting with nuclei in the earth's atmosphere. These reactions produce pions which, in turn undergo the following decay

$$\pi^\pm \rightarrow \mu^\pm + \nu_\mu(\bar{\nu}_\mu),$$

followed by

$$\mu^\pm \rightarrow e^\pm + \nu_e(\bar{\nu}_e) + \bar{\nu}_\mu(\nu_\mu).$$

One observes that there are twice as many muon type of neutrinos as that of the electron type. (Unless explicitly stated, in this section we call neutrinos and anti-neutrinos collectively as neutrinos). There are detailed Monte Carlo predictions for these fluxes, and they confirm that the ratio of the flux of muon neutrinos Φ_{ν_μ} to the flux of electron neutrinos Φ_{ν_e} is about 2 [17,18]. The absolute neutrino fluxes predicted from different calculations however differ significantly from each other (by as much as 30%), but the predictions for the ratio of the fluxes $\Phi_{\nu_\mu}/\Phi_{\nu_e}$ are in good agreement with each other (to within 5%). This is because though the individual fluxes have large uncertainties, this cancels out in the prediction of the ratio. The large water Cerenkov detectors Kamiokande and IMB [19] have measured this ratio and have found it to be about half of what is predicted [20]. This anomalous value of the ratio is called ‘the atmospheric neutrino problem’. The experimental results are presented in the form of a double ratio

$$R = \frac{\left(\frac{N_{\nu_\mu}}{N_{\nu_e}}\right)_{\text{obs}}}{\left(\frac{N_{\nu_\mu}}{N_{\nu_e}}\right)_{\text{MC}}} = \frac{r_{\text{obs}}}{r_{\text{MC}}}. \quad (17)$$

N_{ν_μ} is the number of events which are induced by muon type of neutrinos, while N_{ν_e} is the number of events induced by electron type of neutrinos. The suffix ‘obs’ stands for the observed number of events, while ‘MC’ stands for the Monte Carlo prediction. Kamiokande collaboration have presented their results for neutrinos with energy less than 1.33 GeV (sub-GeV data) [2] and for neutrinos with energy greater than 1.33 GeV (multi-GeV data) [3]. For the sub-GeV data, $R = 0.60^{+0.07}_{-0.06} \pm 0.05$ and for the multi-GeV data, $R = 0.57^{+0.08}_{-0.07} \pm 0.07$ after averaging over the zenith angle. Here the zenith angle denoted by θ is the angle between the direction of the incident neutrino, and the vertical axis passing through the detector. As the detector is located about a few km below the surface of the earth, $\theta = 0^\circ$, means the neutrinos are coming straight from above, and $\theta = 180^\circ$ means the neutrinos are coming from below, i.e., neutrinos which travel the whole diameter of the earth to reach the detector (note the downward direction is taken as the positive zenith axis). The value of R has no significant zenith angle dependence for the sub-GeV data. However, for the multi-GeV data, R is small for large values of zenith angle (upward going neutrinos) and is large for small values of zenith angle (downward going neutrinos). Also the number of electron neutrino events alone are in reasonable agreement with data, while there is an appreciable deficit of the muon neutrino events.

3.1 Three flavor analysis

The transformation between the flavor and the mass eigenstates is given by U^v defined earlier. Now, if $\delta_{21} \sim 10^{-6}\text{eV}^2$, the oscillation length corresponding to it, even for the minimum of the atmospheric neutrino energies, is much larger than the length scales associated with the atmospheric neutrino problem. So δ_{21} is redundant for the atmospheric neutrino problem and can be set to zero. Given this it has been demonstrated that the (12) mixing angle ω does not appear in the oscillation probabilities [21]. Hence it can be set equal to zero. We also neglect CP violation, and set the CP violating phase to zero. Hence the atmospheric neutrino problem is also a function of three parameters, viz ψ , ϕ and δ_{31} .

Including matter effects we get the mixing angles and mass eigenvalues in matter. The mixing angle ψ remains unaffected but the angle ϕ becomes matter dependent. We obtain [21],

$$\tan 2\phi_m = \frac{\delta_{31} \sin 2\phi}{\delta_{31} \cos 2\phi - A}, \quad (18)$$

and

$$\psi_m = \psi. \quad (19)$$

The mass eigenvalue of ν_1^m remains 0 (actually it is of the order of δ_{21} which we are neglecting here). The other two matter dependent mass eigenvalues are given by

$$m_2^2 = \frac{1}{2} \left[(\delta_{31} + A) - \sqrt{(\delta_{31} \cos 2\phi - A)^2 + (\delta_{31} \sin 2\phi)^2} \right], \quad (20)$$

$$m_3^2 = \frac{1}{2} \left[(\delta_{31} + A) + \sqrt{(\delta_{31} \cos 2\phi - A)^2 + (\delta_{31} \sin 2\phi)^2} \right]. \quad (21)$$

Equations (18), (20) and (21) are valid for neutrinos. For anti-neutrinos, we get a similar set of formulae with A replaced by $-A$. The neutrinos produced in the atmosphere enter the earth after travelling through the atmosphere for about 20 km and finally reach the detector after travelling through the earth. The distance travelled through the earth is a function of the zenith angle. For the five bins considered by Kamiokande [3], the average values of the cosine of the zenith angle are $-0.8, -0.4, 0.0, 0.4, 0.8$ and the average distances travelled through the earth are 10210, 5137, 832, 34, 6 km respectively [22].

A neutrino of flavor α , produced in the atmosphere at time $t = 0$, propagates through the atmosphere as a linear combination of the vacuum mass eigenstates. If the neutrino enters earth at time $t = t_1$, its state vector at that time can be written as

$$|\Psi_\alpha(t_1)\rangle = \sum_i U_{\alpha i}^v \exp\left(-i\frac{\mu_i^2 t_1}{2E}\right) |\nu_i^v\rangle. \quad (22)$$

Re-expressing the vacuum mass eigenstates in terms of flavor states, we have

$$|\Psi_\alpha(t_1)\rangle = \sum_i U_{\alpha i}^v \exp\left(-i\frac{\mu_i^2 t_1}{2E}\right) \sum_\lambda U_{\lambda i}^{v*} |\nu_\lambda\rangle. \quad (23)$$

After entering the earth, the neutrino propagates as a linear combination of the matter dependent mass eigenstates. We take the earth to be a slab of constant density. At the time of detection $t = t_d$, the state vector takes the form

$$\begin{aligned} |\Psi_\alpha(t_d)\rangle &= \sum_i U_{\alpha i}^v \exp\left(-i\frac{\mu_i^2 t_1}{2E}\right) \sum_\lambda U_{\lambda i}^{v*} \sum_j U_{\lambda j}^m \\ &\times \exp\left(-i\frac{m_j^2(t_d - t_1)}{2E}\right) |\nu_j^m\rangle. \end{aligned} \quad (24)$$

Hence the amplitude for the neutrino produced as flavor α at $t = 0$ to be detected as a neutrino of flavor β at time t_d is given by

$$\begin{aligned} \langle \nu_\beta | \Psi_\alpha(t_d) \rangle &= \sum_{i,j} \sum_{\lambda} U_{\alpha i}^v U_{\lambda i}^{v*} U_{\lambda j}^m U_{\beta j}^{m*} \exp\left(-i \frac{\mu_i^2 t_1}{2E}\right) \\ &\times \exp\left(-i \frac{m_j^2(t_d - t_1)}{2E}\right). \end{aligned} \quad (25)$$

The probability of oscillation $P_{\alpha\beta}$ is given by the modulus square of the above amplitude. If $t_d - t_1$ is set equal to zero (that is if the total time of travel is equal to the time of travel through the atmosphere) then the expression in eq. (25) reduces to the simple vacuum oscillation amplitude. The same is true if the matter effects are ignored, i.e., if $U^m = U^v$ and $m_i = \mu_i$.

3.2 Analysis

We refer to ref. [23] for details of our calculation. Below we give the salient features of our analysis.

1. *Sub-GeV data*: First we describe our analysis of the sub-GeV data. Matter effects are unimportant for the sub-GeV data. If the earth is taken to be a slab of density 5.5 gm/cm^3 , the matter term A for the sub-GeV neutrinos is less than $3.8 \times 10^{-4} \text{ eV}^2$. As we will shortly see, the sub-GeV data sets a lower limit on $\delta_{31} > 10^{-3} \text{ eV}^2$. Hence the matter effects can be neglected and the expressions for $P_{\alpha\beta}$ in the sub-GeV analysis are simply the vacuum oscillation probabilities

$$\begin{aligned} P_{\alpha\beta}^0 &= (U_{\alpha 1}^v U_{\beta 1}^v)^2 + (U_{\alpha 2}^v U_{\beta 2}^v)^2 + (U_{\alpha 3}^v U_{\beta 3}^v)^2 \\ &+ 2 U_{\alpha 1}^v U_{\alpha 2}^v U_{\beta 1}^v U_{\beta 2}^v \cos\left(2.53 \frac{d \delta_{21}}{E}\right) \\ &+ 2 U_{\alpha 1}^v U_{\alpha 3}^v U_{\beta 1}^v U_{\beta 3}^v \cos\left(2.53 \frac{d \delta_{31}}{E}\right) \\ &+ 2 U_{\alpha 2}^v U_{\alpha 3}^v U_{\beta 2}^v U_{\beta 3}^v \cos\left(2.53 \frac{d \delta_{32}}{E}\right), \end{aligned} \quad (26)$$

where d is the distance of travel in meters, δ 's are the mass differences in eV^2 and E is the neutrino energy in MeV. Because we have neglected the CP violating phase, the oscillation probability for the anti-neutrinos is the same as that for the neutrinos. Since δ_{21} is very small, the cosine term containing it in eq. (26) can be set equal to 1. The other two cosine terms are dependent on δ_{31} (and $\delta_{32} \simeq \delta_{31}$), the neutrino energy and the distance of travel which is related to the zenith angle. As mentioned earlier, the double ratio R defined in eq. (17) does not have any zenith angle dependence for the sub-GeV data. One can account for this if it is possible to replace the distance dependent terms in eq. (26) by their average values. This replacement is possible only if the average distance travelled contains many oscillation lengths. The above condition sets a lower limit on the mass difference

$\delta_{31} > 10^{-3} \text{ eV}^2$ [29]. Note that this lower limit is consistent with the approximation $\delta_{31} \gg \delta_{21} \sim 10^{-5} \text{ eV}^2$, which was made so that both solar and atmospheric neutrino problems could be solved simultaneously.

The expression for R can simply be written as

$$R = \frac{P_{\mu\mu}^0 + \frac{1}{r_{MC}} P_{e\mu}^0}{P_{ee}^0 + r_{MC} P_{\mu e}^0}, \quad (27)$$

where

$$r_{MC} = \frac{\int [\phi_{\nu_\mu} \sigma_\mu + \phi_{\bar{\nu}_\mu} \sigma_{\bar{\mu}}] dE}{\int [\phi_{\nu_e} \sigma_e + \phi_{\bar{\nu}_e} \sigma_{\bar{e}}] dE}, \quad (28)$$

where r_{MC} is the Monte Carlo expectation of the ratio of number μ -like events to the number of e -like events. From the sub-GeV data of Kamiokande, we find $r_{MC} = 1.912$ and $R = 0.60_{-0.06}^{+0.07} \pm 0.05$ [2]. We take the allowed values of ϕ from our analysis of solar neutrino data which restricts ϕ to be in the range $0 \leq \phi \leq 50^\circ$ [7]. We find the allowed region in the $\phi - \psi$ plane by requiring the theoretical value calculated from eq. (27) to be within 1σ or 1.6σ uncertainty of the experimental value. The region allowed by the sub-GeV data, where ϕ was restricted by the solar neutrino data and ψ is allowed to vary between 0 to 90° , is shown in figure 2. The region between the solid lines is the parameter space which satisfies the experimental constraints at 1σ level whereas the region between dashed lines satisfies the experimental constraints at 1.6σ level. One important point to be noted in this analysis is that the sub-GeV data place only lower bound on δ_{31} . The allowed region in $\phi - \psi$ plane is quite large.

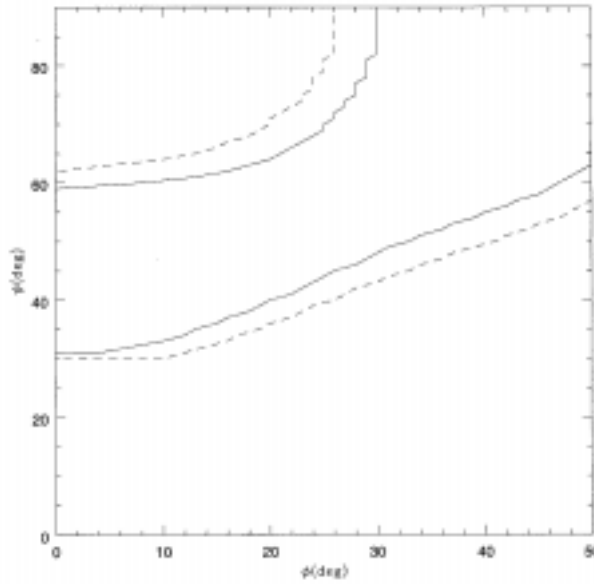


Figure 2. Allowed region in $\phi - \psi$ plane by the sub-GeV data (with $\delta_{31} \geq 10^{-3} \text{ eV}^2$) at 1σ (enclosed by solid lines) and at 1.6σ (enclosed by broken lines).

Table 1. Zenith angle dependent data from Kamiokande (3).

Bin no.	$\langle \cos \theta \rangle$	$\langle \text{distance} \rangle$ in km	r_{MC}^i	r_{obs}^i	R_{obs}^i
1	-0.8	10,210	3.0	$0.87^{+0.36}_{-0.21}$	$0.29^{+0.12}_{-0.07}$
2	-0.4	5,137	2.3	$1.06^{+0.39}_{-0.30}$	$0.46^{+0.17}_{-0.13}$
3	0.0	832	2.1	$1.07^{+0.32}_{-0.23}$	$0.51^{+0.15}_{-0.11}$
4	0.4	34	2.3	$1.45^{+0.51}_{-0.34}$	$0.63^{+0.22}_{-0.16}$
5	0.8	6	3.0	$3.9^{+1.8}_{-1.2}$	$1.3^{+0.6}_{-0.4}$

2. *Multi-GeV data:* The multi-GeV data of Kamiokande have been presented for five zenith angle bins in ref. [3]. For each of these bins, the observed numbers of electron-like events and muon-like events and their Monte Carlo expectations (without neutrino oscillations) have been given. From these one can calculate two sets of ratios

$$r_{\text{MC}}^i = \left(\frac{N_{\mu}^i}{N_e^i} \right)_{\text{MC}}, \quad (29)$$

$$r_{\text{obs}}^i = \left(\frac{N_{\mu}^i}{N_e^i} \right)_{\text{obs}}, \quad (30)$$

and the set of double ratios

$$R_{\text{obs}}^i = r_{\text{obs}}^i / r_{\text{MC}}^i \quad (31)$$

for each bin $i = 1, 2, \dots, 5$. We summarize the multi-GeV data of Kamiokande [3] in table 1. In the multi-GeV regime the μ -like events are subdivided into fully contained (FC) and partially contained (PC) events whereas all the e -like events are fully contained. The efficiency of detection for each type of event is different and is a function of the neutrino energy. This must be taken into account in the analysis [24].

We can calculate the ratio of μ -like events to e -like events in the presence of oscillations to be

$$r_{\text{osc}}^i = \left(\frac{N_{\mu}^i}{N_e^i} \right)_{\text{osc}} \quad (32)$$

and the double ratio

$$R_{\text{osc}}^i = \frac{r_{\text{osc}}^i}{r_{\text{MC}}^i}. \quad (33)$$

3.3 Results and conclusions

If the atmospheric neutrino deficit is due to neutrino oscillations, then the double ratios R_{osc}^i given in eq. (33) should be within the range of the corresponding observed double ratios R_{obs}^i , which are given in table 1. We searched for the values of the neutrino parameters

ϕ , ψ and δ_{31} for which the predicted values of R_{osc}^i satisfy the experimental constraints on the double ratios for all the five bins. The ranges of variation in the three parameters are:

1. $0 \leq \phi \leq 50^\circ$. This is the range of ϕ allowed by the solar neutrino problem. For this range of ϕ , there exist values of δ_{21} and ω such that all the three solar neutrino experiments can be explained [7,16].
2. $0 \leq \psi \leq 90^\circ$. ψ is varied over its fully allowed range.
3. $10^{-3} \text{ eV}^2 \leq \delta_{31} \leq 10^{-1} \text{ eV}^2$. The lower limit is given by the sub-GeV data and the upper limit is the largest value allowed by the two flavor analysis of the multi-GeV data by Kamiokande [3].

The results are plotted in figures 3 and 4. Figure 3 gives the projection of the allowed region on the ϕ - ψ plane and figure 4 gives the projection on the ψ - δ_{31} plane. The solid lines enclose the regions of parameter space whose predictions lie within the experimental range given by 1σ uncertainties. The broken lines enclose regions whose predictions fall within the range given by 1.6σ uncertainties. These results have been presented in [23]. The salient features of the results of the multi-GeV analysis are:

- Most of the parameter space allowed by the multi-GeV data is a subset of the space allowed by the sub-GeV data.

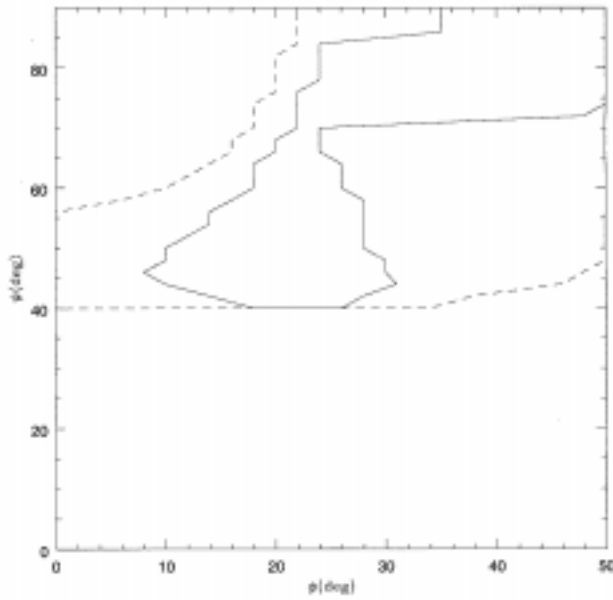


Figure 3. Allowed region in ϕ - ψ plane by 5 bin analysis of multi-GeV data (with $10^{-3} \text{ eV}^2 \leq \delta_{31} \leq 10^{-1} \text{ eV}^2$) at 1σ (enclosed by solid lines) and at 1.6σ (enclosed by broken lines).

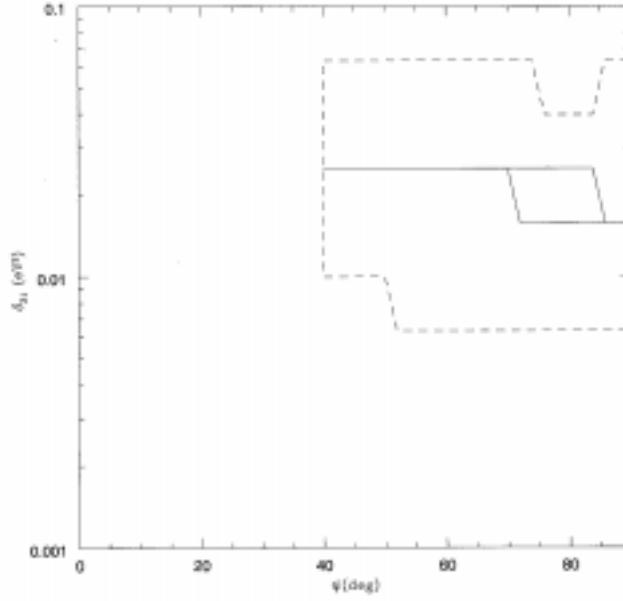


Figure 4. Allowed region in $\phi - \psi$ plane by 5 bin analysis of multi-GeV data (with $0 \leq \phi \leq 50^\circ$) at 1σ (enclosed by solid lines) and at 1.6σ (enclosed by broken lines).

- The range of δ_{31} allowed by 1σ vetoes is extremely narrow. It is very close to the best fit value given by the two flavor analysis of Kamiokande.
- The value of ψ is always large ($\psi \geq 40^\circ$) and $\psi = 90^\circ$ is allowed.
- In the region allowed by 1σ vetoes ϕ is always non-zero. $\phi = 0$ is allowed only at 1.6σ vetoes.

From the parametrization of U^v , effective two level mixings can be obtained for the following choices of the angles:

- $\nu_e \leftrightarrow \nu_\mu$ for $\psi = 90^\circ$,
- $\nu_e \leftrightarrow \nu_\tau$ for $\psi = 0$ and
- $\nu_\mu \leftrightarrow \nu_\tau$ for $\phi = 0$.

Any solution to the atmospheric neutrino problem should suppress the muon neutrinos, enhance the electron neutrinos or do both. The $\nu_e \leftrightarrow \nu_\tau$ channel, which suppresses electron neutrinos but leaves muon neutrinos untouched, cannot account for the atmospheric neutrino problem. Hence any solution of atmospheric neutrino problem should be away from the effective two flavor $\nu_e \leftrightarrow \nu_\tau$ oscillations. The large value of the angle ψ is just a reflection of this fact. The allowed region includes the value $\psi = 90^\circ$. Then the atmospheric neutrino problem is explained purely in terms of the two flavor oscillations between $\nu_e \leftrightarrow \nu_\mu$, with the relevant mass difference being δ_{31} . In this case, the solar neutrino problem is solved by $\nu_e \rightarrow \nu_\tau$ oscillation which is determined by the mass difference δ_{21} (and the mixing angles ω and ϕ).

How important are the matter effects in the analysis of the multi-GeV data? It can be seen from figures 2(d)–(f) of ref. [3] that most of the expected multi-GeV events are caused by neutrinos with energies less than 10 GeV (over 80% for muon-like events and over 90% for electron-like events). The matter term, for a neutrino of energy 5 GeV, is about $2 \times 10^{-3} \text{eV}^2$. Since the initial range we considered for δ_{31} varied from 10^{-3}eV^2 to 0.1eV^2 , *a priori* one must include the matter effects in the expressions for the oscillation probabilities. However, the value of δ_{31} in the allowed region, especially for the 1σ vetoes, where it is about 0.03eV^2 , is much larger than the matter term. Therefore, it is likely that the matter effects may not play an important role in determining the allowed parameter regions in the analysis of the multi-GeV data. To check this we reran our program with the matter term set equal to zero. With this change, the double ratio R_{osc}^i , defined in eq. (32), changes by about 10% in the first bin and by about 5% in the second bin. There is no discernible change in the other three bins. Since the errors in R_{obs}^i are about 30%, these small changes in R_{osc}^i do not lead to any appreciable change in the allowed regions of the parameter space. However, the effect of matter terms may become discernible when more accurate data from super-Kamiokande become available.

Since the earth matter effects seem to play no role in the determination of the parameter space, can one interpret the observed zenith angle dependence purely in terms of vacuum oscillations? For an energy of 5 GeV, the mass square difference 10^{-2}eV^2 corresponds to an oscillation length of about 1200 km. Thus bins 1 and 2 contain many oscillation lengths and the second and the third cosine terms in the vacuum oscillation probability, given in eq. (26), average out to zero. For bins 4 and 5 the cosine terms are almost 1. In bin 3, these terms take some intermediate value. Therefore we have large suppression in the first two bins, almost no suppression in the last two bins and moderate suppression in the middle bin. In conclusion, we have analysed the atmospheric neutrino data of Kamiokande in the context of three flavor neutrino oscillations. We found that the matter effects have negligible influence on atmospheric neutrinos even in the multi-GeV range. The atmospheric neutrino problem enables us to put bounds on the two neutrino parameters which are unconstrained by solar neutrino data.

Super-Kamiokande have also published their results on atmospheric neutrino events, and a comprehensive three flavor analysis of their results is given in [25]. Super-Kamioka results favor a smaller range of δ_{31} as compared to Kamioka. The best fit point for δ_{31} is an order of magnitude lower than that for Kamioka. The (23) mixing angle ψ is still maximum i.e 45 degrees. An important aspect of super-Kamioka results is that there is hardly any change in the observed spectrum of electron events vis-a-vis the Monte Carlo expectation. But this by itself does not restrict the mixing angle ϕ to be small, i.e super-Kamioka data does not constrain ϕ to be small [26]. So large values of ϕ are allowed by super-Kamioka data.

4. Constraints from reactor and accelerator based experiments

Neutrino oscillation experiments with laboratory beams can be broadly classified into short baseline and long baseline experiments. In a short baseline experiment the source to detector distance is typically less than 1 km. For the long baseline experiments the distance is hundreds of km. The survival probability, i.e the probability that the neutrino retains its original flavor denoted by P_{ee} (we consider electron neutrinos and only two flavors as an

example) after traveling a distance x is given by

$$P_{ee} = 1 - \sin^2 2\theta \sin^2 \left(\frac{\delta m^2}{4E} x \right).$$

In usual units the formula for P_{ee} can be written as

$$P_{ee} = 1 - \sin^2 2\theta \sin^2 \left(\frac{1.27 \delta m^2 (\text{eV}^2) x (m)}{E (\text{MeV})} \right) \quad (34)$$

and

$$P_{e\mu} = \sin^2 2\theta \sin^2 \left(\frac{1.27 \delta m^2 (\text{eV}^2) x (m)}{E (\text{MeV})} \right), \quad (35)$$

where the distance x is measured in meters, δm^2 in eV^2 and E is in MeV.

One sees from the above two equations that for a given value of δm^2 and $\sin^2 2\theta$, the sensitivity of a baseline experiment to possible oscillations is controlled by the factor x/E . Example if δm^2 is very small, then one needs large values of x/E to observe oscillations with fine tuning. All the laboratory experiments performed so far (with one exception which we shall discuss soon) have been short baseline experiments. For a review see [27]. The range of x/E accessible to these experiments has been from about $10^{-2} - 10$ (in units of $m \text{ MeV}^{-1}$). None of these experiments has found any evidence for neutrino oscillations. Very recently the CHOOZ collaboration [28], a reactor based experiment which searches for signals of $\bar{\nu}_e \rightarrow \bar{\nu}_x$ oscillations, where x can be any other flavor, in the disappearance mode of the original flavor has reported the results of its first run [28]. Even though the source to detector distance for CHOOZ is only about 1 km, it mimics a long baseline experiment. This is because the beam energy being very low ($\approx 3 \text{ MeV}$) the average value of x/E is equal to 300. Hence it can probe mass squared differences as low as 10^{-3} eV^2 , an order of magnitude lower than previous reactor experiments. The collaboration sees no evidence of oscillations of the original flavor. They have analysed their results assuming two flavor oscillations between ν_e and another flavor and gave an exclusion plot in the parameter space spanned by the mass squared difference Δm^2 and the mixing angle θ . Their main result is that for $\Delta m^2 > 3 \times 10^{-3} \text{ eV}^2$, $\sin^2(2\theta)$ must be less than 0.18 [28].

4.1 Three flavor analysis of CHOOZ result

In three flavors the vacuum oscillation probability for a neutrino of flavor α to oscillate into a neutrino of flavor β is given by

$$\begin{aligned} P_{\alpha\beta}^0 = & (U_{\alpha 1} U_{\beta 1})^2 + (U_{\alpha 2} U_{\beta 2})^2 + (U_{\alpha 3} U_{\beta 3})^2 \\ & + 2 U_{\alpha 1} U_{\alpha 2} U_{\beta 1} U_{\beta 2} \cos \left(2.53 \frac{d \delta_{21}}{E} \right) \\ & + 2 U_{\alpha 1} U_{\alpha 3} U_{\beta 1} U_{\beta 3} \cos \left(2.53 \frac{d \delta_{31}}{E} \right) \\ & + 2 U_{\alpha 2} U_{\alpha 3} U_{\beta 2} U_{\beta 3} \cos \left(2.53 \frac{d \delta_{32}}{E} \right), \end{aligned} \quad (36)$$

where d is the distance traveled in meters, E is in MeV, and mass squared differences are in eV^2 . We may also note the vacuum oscillation probabilities are same as in eq. (36) for the case of antineutrinos because CP violation is neglected. If we assume the hierarchy among the neutrino mass eigenstates $\delta_{31} \gg \delta_{21}$, and that δ_{21} is about 10^{-5}eV^2 , which is required to fit solar neutrino data [1], then the oscillatory term involving δ_{21} can be set to one. The oscillation probability relevant for the CHOOZ experiment is the electron neutrino survival probability P_{ee} which is easily computed from eq. (36) to be

$$P_{ee} = 1 - \sin^2 2\phi \sin^2 \left(1.27 \frac{d\delta_{31}}{E} \right). \quad (37)$$

Notice the interesting point that this involves only the (13) mixing angle ϕ , and because of the hierarchy the (12) mixing angle ω disappears from the probability. So we reinterpret the CHOOZ result [28], to be that for $\delta_{31} > 3 \times 10^{-3}$, $\sin^2(2\phi)$ must be less than 0.18, i.e $\phi < 12.5^\circ$. At this point we wish to emphasize again the importance of a three flavor analysis. The fact is that the (13) mixing angle which is constrained by CHOOZ can be seen only in a three flavor analysis [29]. We can now estimate the maximum contribution of the $e - \mu$ channel to the atmospheric neutrino anomaly using the CHOOZ result. Since the relevant δ_{31} is about 10^{-2}eV^2 , matter effects are negligible for the problem [23]. Hence the relevant probability is the vacuum $\nu_e \leftrightarrow \nu_\mu$ oscillation probability,

$$P_{\bar{\mu}e} = P_{\mu e} = \sin^2 2\phi \sin^2 \psi \sin^2 \left(1.27 \frac{d\delta_{31}}{E} \right). \quad (38)$$

Note that both ϕ and ψ have to be non-zero for $P_{\mu e}$ to be non-zero, and also the oscillation length corresponding to δ_{21} does not contribute to the atmospheric neutrino problem [23]. Now solutions to Kamiokande atmospheric neutrino data [23,29] require a value of $\psi \geq 45^\circ$. The average contribution of the oscillatory term is 0.5. Therefore using the CHOOZ result that the maximum value of $\sin^2(2\phi)$ allowed is 0.18 we get

$$P_{\mu e}^{\text{max}} \leq 1.0 \times 0.18 \times 0.5 = 0.09 \quad (39)$$

which is less than 9 per cent. Hence the atmospheric neutrino anomaly is driven almost completely by $\nu_\mu \leftrightarrow \nu_\tau$ oscillations. This bears out our previous analysis of the atmospheric neutrino problem [23]. We found that matter effects play a negligible role in the solution to even binned multi-GeV data. Hence the θ dependence of data can be simply explained by the distance dependence of various oscillation probabilities. In three flavors since ν_e can oscillate into ν_τ also we compute the $e - \tau$ conversion. The $\nu_e \leftrightarrow \nu_\tau$ conversion probability is given by

$$P_{\bar{e}\tau} = P_{e\tau} = \sin^2 2\phi \cos^2 \psi \sin^2 \left(1.27 \frac{d\delta_{31}}{E} \right). \quad (40)$$

Since $\psi > 45^\circ$, we find that the $e - \tau$ conversion probability is less than 5 per cent, i.e there is very little $e - \tau$ oscillations. Therefore the electron neutrino flux is more or less close to the Monte Carlo (no oscillations) prediction, which is what is experimentally observed.

In figure 5, the light contours enclose the parameter region in $\phi - \psi$ plane allowed by the sub-GeV data of Kamiokande with 1.6σ error bars. The present CHOOZ constraint has been shown as a thick vertical line, with the region to the right of it being excluded.

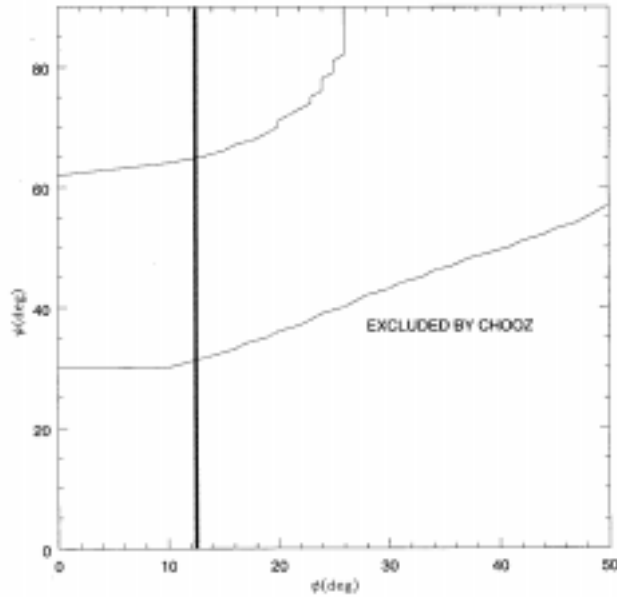


Figure 5. Allowed region in $\phi - \psi$ plane by the sub-GeV data.

One sees that the CHOOZ constraint as properly interpreted in a three flavor framework drastically cuts into the parameter space which was previously allowed. Now observe what is probably the most important consequence of the CHOOZ result. The fact that ϕ , the link between the solar and the atmospheric neutrino problems is constrained to be small implies that the solar neutrino problem can be essentially viewed as a two flavor $\nu_e \leftrightarrow \nu_\mu$ oscillation phenomena, and the atmospheric neutrino problem essentially as a two flavor $\nu_\mu \leftrightarrow \nu_\tau$ oscillation phenomena even in a three flavor framework. We mention that this remarkable result implies that for the solar neutrino problem there is essentially only the small angle and the large solutions. See figure 1 where the parameter space for $\phi = 10^\circ$ is shown. There is no discernible change as compared to the $\phi = 0^\circ$ case. We mention in passing that in three flavors, the larger mass scale, i.e δ_{31} in our case cannot account for atmospheric plus CHOOZ plus LSND results.

5. Conclusions

A minimum of three neutrino flavors are needed to simultaneously explain the solar and the atmospheric neutrino problems. The present data from solar and atmospheric neutrino experiments give a large region in the three flavor parameter space. This region is drastically reduced if one incorporates the result of the recent CHOOZ long baseline experiment on the parameter space. The CHOOZ result also demonstrates the decoupling of the solar and the atmospheric neutrino problems from each other. The solar neutrino parameter space is effectively reduced to the usual two flavor small angle and large angle solutions. Future experiments mainly BOREXINO and SNO will enable us to distinguish between the large and the small angle solutions.

Acknowledgements

I thank the organizers of this meet for giving me the opportunity to present our results.

References

- [1] N Hata and P Langacker, *Phys. Rev.* **D56**, 6107 (1997)
- [2] Kamiokande Collaboration: K S Hirata *et al*, *Phys. Lett.* **B280**, 146 (1992)
- [3] Kamiokande Collaboration: Y Fukuda *et al*, *Phys. Lett.* **B335**, 237 (1994)
- [4] T K Kuo and J Pantaleone, *Rev. Mod. Phys.* **61**, 937 (1989)
- [5] T K Kuo and J Pantaleone, *Phys. Rev.* **D35**, 3432 (1987)
- [6] A S Joshipura and M V N Murthy, *Phys. Rev.* **D37**, 1374 (1988)
- [7] M Narayan, M V N Murthy, G Rajasekaran and S Uma Sankar, *Phys. Rev.* **D53**, 2809 (1996)
- [8] L D Landau and E M Lifshitz, *Non-relativistic Quantum Mechanics*, 3rd Edition (Pergamon Press, 1977)
- [9] GALLEX Collaboration: M Cribier, in TAUP' 97 5th International Workshop on Topics in Astroparticle and Underground Physics (Laboratori Nazionali del Gran Sasso, Assergi, Italy, 1997) to appear in the proceedings
- [10] SAGE Collaboration: in LP'97, 28th International Symposium on Lepton Photon Interactions (Hamburg, Germany, 1997) to appear in the proceedings
- [11] Homestake Collaboration: K Lande, in the 4th international Solar Neutrino conference (Heidelberg, Germany, 1997) to appear in the proceedings
- [12] Kamiokande Collaboration: Y Fukuda *et al*, *Phys. Rev. Lett.* **77**, 1683 (1996)
- [13] Super-Kamioka Collaboration: Y Totsuka, in LP'97, 28th International Symposium on Lepton Photon Interactions (Hamburg, Germany, 1997) to appear in the proceedings
- [14] J N Bahcall and M H Pinsonneault, *Rev. Mod. Phys.* **67**, 781 (1995)
- [15] J Bahcall, *Neutrino Astrophysics* (Cambridge University Press)
- [16] G Fogli, E Lisi and D Montanino, *Phys. Rev.* **D49**, 3626 (1994); *ibid.* **D54**, 2048 (1996)
- [17] M Honda *et al*, *Phys. Rev.* **D52**, 4985 (1995)
- [18] Agrawal *et al*, *Phys. Rev.* **D53**, 1314 (1996)
- [19] IMB Collaboration: D Casper *et al*, *Phys. Rev. Lett.* **66**, 2561 (1991)
R Becker-Szendy *et al*, *Phys. Rev.* **D46**, 3720 (1992)
- [20] IMB Collaboration observed a deficit of muon-like events in their data compared to the Monte-Carlo prediction as early as 1986 and have speculated whether this deficit is due to non-standard physics
T J Haines *et al*, *Phys. Rev. Lett.* **57**, 1986 (1986)
- [21] J Pantaleone, *Phys. Rev.* **D49**, R2152 (1994)
- [22] C Giunti, C W Kim and J D Kim, *Phys. Lett.* **352B**, 357 (1995)
- [23] M Narayan, G Rajasekaran and S Uma Sankar, *Phys. Rev.* **D56**, 437 (1997)
- [24] We thank Prof. T Kajita of the Kamiokande Collaboration for providing us with the efficiencies for the detection of various types of events
- [25] G Fogli, E Lisi and A Marrone and G Scioscia, *Phys. Rev.* **D59**, 033001 (1999)
- [26] J Pantaleone, *Phys. Rev. Lett.* **81**, 5060 (1998)
- [27] L Oberauer and F von Feilitzsch, *Rep. Prog. Phys.* **55**, 1093 (1992)
- [28] The CHOOZ Collaboration: M Apollonio *et al*, *Phys. Lett.* **B420**, 397 (1998) (Initial results from the CHOOZ long baseline reactor neutrino oscillation experiment)
- [29] Mohan Narayan, G Rajasekaran, and S Uma Sankar *Phys. Rev.* **D58**, R031301 (1998)